2021

The effect of uneven heating on the flow distribution between parallel microchannels undergoing boiling

A. Miglani

A. Soto

J.A. Weibel

S.V. Garimella

Miglani, A.; Soto, A.; Weibel, J.A.; and Garimella, S.V., "The effect of uneven heating on the flow distribution between parallel microchannels undergoing boiling" (2021). *CTRC Research Publications.* Paper 380.
http://dx.doi.org/10.1115/1.4052532

The effect of uneven heating on the flow distribution between parallel microchannels undergoing boiling

Ankur Miglani[a, b], Anali Soto[a], Justin Weibel[a*] and Suresh V. Garimella[a**]

[a]*School of Mechanical Engineering, Purdue University, West Lafayette, IN 47907 USA*

[b]*Department of Mechanical Engineering, Indian Institute of Technology, Indore, Madhya Pradesh 453552, India*

Abstract:

As the size, weight, and performance requirements of electronic devices grow increasingly demanding, their packaging has become more compact. As a result of thinning or removing the intermediate heat spreading layers, non-uniform heat generation from the chip-scale and component-level variations may be imposed directly on the attached microchannel heat sink. Despite the important heat transfer performance implications, the effect of uneven heating on the flow distribution in parallel microchannels undergoing boiling has been largely unexplored. In this study, a two-phase flow distribution model is used to investigate the impact of uneven heating on the flow distribution behavior of parallel microchannels undergoing boiling. Under lateral uneven heating (*i.e.*, the channels are each heated to different levels, but the power input is uniform along the length of any given channel), it is found that the flow is significantly more maldistributed compared to the even heating condition. Specifically, the range of total flow rates over which the flow is maldistributed is broader and the maximum severity of flow maldistribution is higher. These trends are assessed as a function of the total input power, degree of uneven heating, and the extent of thermal connectedness between the channels. The model predictions are validated against experiments for a representative case of thermally isolated and coupled channels subjected to even heating and extreme lateral uneven heating conditions and show excellent agreement.

Keywords: Flow boiling; Flow distribution; Uneven heating; Parallel microchannels; Thermal coupling; Two-phase flow

* Corresponding author: jaweibel@purdue.edu

**Currently President, University of Vermont

1. Introduction

Modern high-performance electronic devices feature high power densities and compact packages where it is not always feasible or beneficial to introduce thick intermediate heat spreaders to spread out the non-uniform heat generation profiles. Instead, the attached heat sink may experience the non-uniform heat flux that result from chip-scale variations or multiple discrete devices in the package [1-6]. Two phase microchannel heat sinks are an attractive solution to dissipate high power densities because of their ability to reduce both the temperature and the temperature gradient in the device while requiring lower pumping power. However, flow boiling in multiple parallel channels is uniquely susceptible to instabilities induced by the heating profile compared to single-phase liquid cooling. Uneven heating can induce unequal flow distribution between the channels, which is undesirable in heat sinks as the channels starved of flow (relative to even flow distribution) may undergo a premature dry-out, thereby impairing their heat transfer performance, and limiting predictability and reliability. While some recent studies have made strides in performance-prediction capabilities [7-9], the state-of-the-art models still assume even flow distribution between microchannels. Therefore, to reliably predict the two-phase cooling performance under realistic heating conditions, it is necessary to understand the impact of uneven heating on the thermal-hydraulic characteristics of boiling flows, especially in terms of the deviation in the heat transfer performance and flow distribution behavior compared to even heating conditions.

Experimental studies in the past have explored the effects of uneven heating on the maximum wall temperatures, pressure drop [2-4], and the flow boiling instabilities in microchannels [5]. For instance, Ritchey et al. [6] studied the effect of location and configuration of local hotspots and different uneven heating profiles (along the streamwise and transverse directions) on the heat sink thermal performance. In all the cases, the wall temperatures and local heat transfer coefficients deviated significantly from even heating conditions. Sarangi et al. [7] developed a numerical model to predict the location of the boiling front, the pressure drop, and the thermal resistance of heated microchannels as a function of the heat input. The model incorporated the effects of axial uneven heating, which showed a significant impact on the overall thermal-hydraulic performance of the system. Revellin et al. [8] predicted the critical heat flux (CHF) in heated microchannels using a one-dimensional theoretical model, and used it to study the effect of size, location, and number of

hot spots as well as the distance between two consecutive hot spots on heat transfer performance [9]. The effects of transient uneven heating on thermal performance of microchannels have also been explored [10-12]. While thermal performance implications of uneven heating have been probed in these studies, the hydrodynamic implications of uneven heating have received less attention (and are not considered in model predictions), even though the observed temperature signatures are often explained based on flow phenomena.

A key hydrodynamic consideration of flow boiling in parallel microchannels is the tendency of the flow to distribute unevenly between the channels. Such flow maldistribution is undesirable in heat sinks as the channels starved of flow (relative to uniform flow distribution) may undergo a premature dry-out and limit the heat transfer performance. Even under uniform heating conditions, flow maldistribution can occur due to the non-monotonic nature of the channel load curve (*i.e.*, channel pressure drop as a function of flow rate), which allows the parallel channels to operate at unequal flow rates even with the same pressure drop. To quantify the flow distribution under even heating conditions, we previously performed direct measurements of the flow rate in two parallel boiling microchannels [13, 14]. Flow rate measurements synchronized with the wall temperature and overall pressure drop were performed to characterize the thermal and hydrodynamic behaviors. The effect of increasing heat load on the flow distribution and difference in parallel channel wall temperatures was studied. When the flow in both channels was in the single-phase liquid regime, the channels had the same wall temperature and received equal flow rates. With increasing power, once boiling occurred in one of the channels, the Ledinegg instability [13, 14] triggered flow maldistribution and a large temperature difference developed between the channels, causing the wall temperature of the flow-starved channel to increase rapidly, deteriorating the heat transfer performance of the system.

Flow distribution characteristics in the parallel channel system are strongly affected by the load curves (pressure drop versus flow rate) of the individual channels [15, 16]. The amount of heat input is one of the key factors that influences the channel load curve because it determines the thermodynamic state of the fluid along the channel at a given flow rate. If the parallel channels have different load curves due to uneven heating, they must then have different flow rates to equilibrate their pressure drops. In this way, uneven heating can induce flow maldistribution in a parallel channel system. A few studies have explored the thermal implications of flow

maldistribution resulting from uneven heating conditions [11,12, 17-19]. For instance, Cho et al. [17] demonstrated that when a hotspot is located close to the heat sink inlet, a large temperature variation is induced across the heat sink in the transverse direction due to the flow maldistribution. Based on the channel wall temperature and overall pressure drop measurements, they inferred that maldistribution resulted from an increase in the local pressure drop due to boiling, which rerouted the inlet sub-cooled liquid flow to other locations. Flynn et al. [18, 19] studied the thermal implications of flow maldistribution in thermally isolated parallel microchannels etched on a silicon substrate. The heat input to the channels was varied independently and they were tested under uneven heating conditions. At high levels of uneven heating, the channel subjected to more heating underwent boiling, while the other remained in single-phase liquid, leading to a noticeable channel-to-channel temperature difference. The existence of flow maldistribution was inferred based on the flow visualizations and temperature measurements. Despite these advances, there has not been a modeling effort with direct comparison to complementary experiments that investigates the effects of operational parameters, such as the varying degree of uneven heating and increasing heat load on the flow maldistribution between parallel microchannels undergoing boiling. Other previous attempts [20-22] to capture the flow maldistribution caused by uneven heating conditions were largely motivated by its occurrence in parallel evaporator channels in large-scale steam generation systems, and therefore, focused on long thermally isolated channels with large diameters, which are not representative of two-phase microchannel heat sinks used in electronics cooling applications.

One important additional consideration is the effect of lateral channel-to-channel thermal coupling (e.g., via heat conduction in a substrate), which acts to mitigate flow maldistribution. When one channel is severely starved of flow and has a higher convective thermal resistance, the heat can redistribute from the flow-starved channel to the neighboring channels and dampen the flow maldistribution [15, 16]. Previous studies [6, 19] have shown that even with very thin substrates beneath the microchannel heat sinks, significant lateral conduction can occur and lead to heat-flux redistribution. Through a combined modeling and experimental approach in our recent study [14], we demonstrated the critical role of thermal coupling in moderating flow maldistribution and enabling temperature equalization under even heating conditions. Quantitative measurement of flow rate in individual channels showed that when the channels are strongly thermally coupled, the range of input power over which the flow maldistribution occurs, and the

maximum severity of flow maldistribution, is significantly reduced compared to thermally isolated channels. Also, no temperature difference exists between the channels due to the heat redistribution via the shared wall and substrate. Therefore, under extreme conditions, when one channel is significantly starved of flow and risks dry out, the channel-to-channel thermal coupling can redistribute the heat load from the flow-starved channel to the channel with excess flow. Due to such a possibility of heat redistribution, coupled channels are significantly less prone to flow maldistribution compared to isolated channels. Despite the known importance and practical relevance of thermal coupling, its effect on the flow distribution behavior under uneven heating conditions has received little attention. The positive role of thermal coupling will assist in the design of heat spreaders that minimize channel-to-channel temperature difference by moderating flow maldistribution and avoid overdesign of the heat spreader.

The objective of this study is to investigate the effect of lateral uneven heating on the flow maldistribution behavior in parallel microchannels undergoing boiling. A two-phase flow distribution model is first used to investigate the flow distribution behavior under lateral uneven heating conditions. Flow distribution behavior is quantified in terms of the range of total flow rates over which maldistribution occurs and the severity of flow maldistribution relative to even heating cases. In addition, a parametric analysis is performed to study the effect of the degree of lateral uneven heating, the heat load, and the thermal coupling between the channels on the severity of flow maldistribution. Finally, the experiments are presented for both thermally isolated channels and thermally coupled channels subject to extreme lateral uneven heating and compared with the model predictions.

2. Model description and cases

The model predictions presented in this study are obtained using the two-phase flow distribution model developed in our previous work [15, 16]. In brief, this modeling approach allows prediction of steady-state flow rate distribution in a system of multiple parallel microchannels undergoing boiling for a subcooled inlet flow. The pressure drop and heat transfer models are developed individually for each channel and then combined into the system flow network along with the pump curve. All possible stable steady-state solutions (*i.e.*, flow distributions) resulting from the system of dynamic flow network equations are determined. The

analysis is based on an ideal, open-loop flow network architecture as shown in Fig. 1. In this flow network the pump delivers sub-cooled liquid to a system of two parallel heated microchannels that are coupled hydraulically via a common inlet and outlet. This ensures that the channels are subjected to identical pressure drop boundary conditions, mimicking the boundary condition for microchannels connected to a common header, as in practical heat sinks.

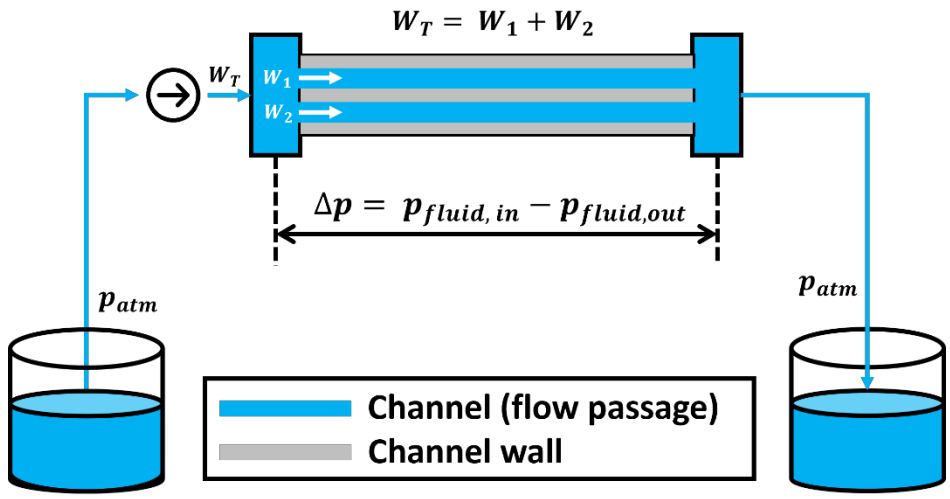

Fig. 1. Schematic diagram of the flow network architecture for a system with flow through two parallel channels

The momentum conservation equation for each channel is given by:

$$K_{channel,i}\frac{dW_i}{dt} = \Delta p - f_{channel,i}(W_i, P_i') \quad (1)$$

This equation governs the temporal variation of flow rate W_i in a channel with index i (=1 or 2). The pressure drop Δp is the instantaneous pressure difference between the inlet and the outlet, which is identical across both channels and is equal to the pressure head provided by the pump. The term $f_{channel,i}(W_i, P_i')$ is the steady-state pressure drop resulting from the hydraulic losses in the channel which is not only a function of flow rate in channel i but depends on the flow rate in the other channel due to the possibility of channel-to-channel heat conduction. The difference between the steady-state pressure drop $f_{channel,i}(W_i, P_i')$ and the overall pressure drop Δp causes the flow rate in a channel to vary with time, and the rate of this variation is dictated by the magnitude of the inertial coefficient of the channel $K_{channel,i}$ (= channel length / cross-sectional

area). The steady-state pressure drop model is formulated based on the separated flow assumption, where the frictional pressure gradient is calculated using the Lockhart-Martinelli method [23].

Mass conservation demands that the total flow rate supplied by the pump W_{total} must equal the sum of flow rates W_i in individual channels with index *i*:

$$W_{total} = \sum_{i=1}^{2} W_i \quad (2)$$

Finally, the pump curve that describes the relationship between the pump flow rate (W_{total}) and the pressure drop (Δp) is given by the following implicit relation:

$$F_{pump}\,(W_{total}, \Delta p) = 0 \quad (3)$$

The heat transfer model for the system includes internal convection in the channels, heat loss to the ambient, and axial and lateral thermal conduction in the solid walls and the substrate. Because lateral thermal conduction plays a critical role in the flow distribution behavior between parallel channels, it was incorporated in the model through the thermal conductance C_{lat}, which quantifies the degree of thermal connectedness between the channels. The lateral thermal conductance (C_{lat}) is defined based on one-dimensional heat conduction between the vertical mid-plane of the channels as $C_{lat} \cong K_{wall} H_b L_c / S_c$ such that a value of C_{lat} = 0 W/K would indicate perfect thermal isolation between the channels. In the model, the value of thermal conductance can be varied to mimic different levels of thermal interaction between the channels and determine the corresponding flow distribution behavior at these levels.

The system of dynamic flow network equations along with the pressure drop model and the heat transfer model describes the flow distribution and pressure drop characteristics of a system with parallel microchannels. The model is solved numerically in MATLAB through a finite-volume discretization of the mass, momentum, and energy conservation (both for fluid and channel wall) equations on a 2D grid with equally sized grid cells or control volumes [16]. The grid represents the footprint area of the microchannel array, where each row corresponds to an individual channel. Since the flow length of each individual channel is discretized along the streamwise direction, any streamwise or lateral heat input profile can be imposed as an input to the model. While the mass conservation is trivially solved, the thermodynamic state of the fluid is determined via the coupled fluid and channel wall energy equations. The pressure drop across each

channel and enthalpy are obtained by numerical integration (trapezoidal rule) of the momentum and energy equations from their respective boundary values, evaluated at the nodes.

The system configuration investigated consists of two adjacent parallel microchannels in a solid substrate. The geometrical parameters of this configuration are adopted from our previous experimental studies [13, 14], while the other set of operational and boundary conditions that are input to the model are detailed in Table 1. The two different heating boundary conditions for which the flow distribution characteristics are analyzed are shown schematically in Fig. 2. The first is a baseline case where the channels are evenly heated with the same input power to both channels (Fig. 2a). In the second case, the channels are subject to uniform heating along each of their lengths but at unequal input powers, thereby resulting in a *lateral uneven heating* condition (Fig. 2b). The flow distribution behavior in each of these cases is analyzed as a function of the input power and thermal conductance between the channels.

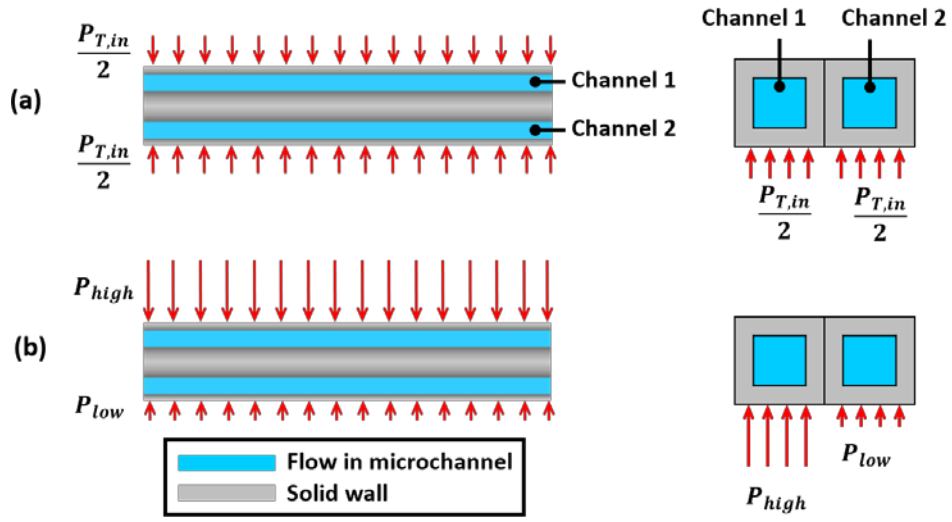

Fig. 2. Schematic diagram of a two-channel system showing different heating conditions analyzed in this study: (a) even heating and (b) lateral uneven heating of the two channels. The top view of the channels is shown on the left. Note that in this view the arrows for input power are shown on the sides only for the purpose of representation. The channels are heated from the bottom as shown in the magnified cross-sectional views on the right.

Table 1. System parameters, operating conditions, and boundary conditions used as model inputs.

Parameters	Magnitude
Channel dimensions: $L_c,\ W_c, H_c\ (mm)$	55, 1, 1
Number of channels	2
Channel block dimensions: $L_b,\ W_b, H_b\ (mm)$	55, 15, 15
Inlet mass flow rate $W_T\ (mg/s)$	0 to 500
Inlet mass flux based on the channel cross-section $m_{in}(\frac{kg}{m^2}-s)$	0 to 500
Fluid inlet temperature $T_{fl,in}$ (℃)	88.5
Outlet pressure $p_{out}\ (kPa)$	104.4
Input power $P_{T,in}$(W)	2.2 W, 4.4 W and 8.8 W
Fluid	Water
Thermal conductivity of channel wall, copper $k_{wall}\ (W/m-K)$	385
Lateral thermal conductance $C_{lat}(W/K)$	0 to 1000
Lateral non-uniformity parameter (φ)	0 to 1

3. Model predictions

This section presents the flow distribution results for a two-channel system subject to the different heating cases described above in Section 2. First, representative results are discussed in Section 3.1 to illustrate the characteristic flow distribution behaviors. These representative results showcase all the relevant features and allow key behaviors to be observed and appropriate metrics defined, such as the range and severity of flow maldistribution, as these will be used in presenting the subsequent cases. This is followed by an investigation of the effect of lateral uneven heating (Section 3.2) on the flow distribution behavior. The effects of different parameters such as the total

input power, degree of uneven heating and the extent of thermal connectedness between channels on the flow distribution characteristics are analyzed.

3.1 Characteristic flow distribution curves

The flow distribution is visualized as a graph of the fraction of flow rate in each channel as a function of the total flow rate, as shown Fig. 3. The flow rate fractions ($\varepsilon_i = W_i/W_T$, where i is the channel index; i = 1, 2) of both channels are shown simultaneously such that their sum equals unity. The flow is uniformly distributed when the flow rate fraction for each channel is 0.5; otherwise, the flow is maldistributed. In a maldistributed condition, most of the flow goes through one channel (referred to as the channel with excess flow) while the flow in the other channel is significantly reduced (referred to as the channel starved of flow). It is important to note that the flow distributions are obtained graphically using the characteristic load curves (non-monotonic pressure drop versus flow rate) of individual channels by simply adding the individual flow rates at a constant pressure drop [15]. Based on the diagrams in Fig. 3, the flow distribution behavior can be characterized in terms of three key metrics, namely, the range of total flow rates over which maldistribution occurs, the most severe flow maldistribution, and the range of total flow rates with this most severe flow maldistribution. The first metric is simply the range of total flow rates over which the channels experience an unequal flow rate. The second metric represents the worst flow distribution where channel 1 has the highest flow rate and channel 2 has the lowest. Both these metrics are marked in Fig. 3. For example, in Fig. 3a, the flow is maldistributed for total flow rates ranging from 50 mg/s to 190 mg/s, and the most severe flow maldistribution results in 97.2% of the flow rate going through channel 1 (channel with excess flow) and 2.8% through channel 2 (flow-starved channel). The third metric represents the range of total flow rates where the flow distribution remains in this most severely maldistributed state (not annotated in the figure). Compared to uniform flow conditions, a maldistributed flow condition is unfavorable as the lack of fluid in the flow-starved channel can lead to dry out and adversely impact the heat transfer performance. Note that in the results presented in Fig. 3 (and throughout the subsequent results) we have arbitrarily defined channel 1 as having the higher flow rate and channel 2 having a lower flow rate. However, when flow maldistribution occurs, it is possible that either channel could have the higher flow rate compared to the other.

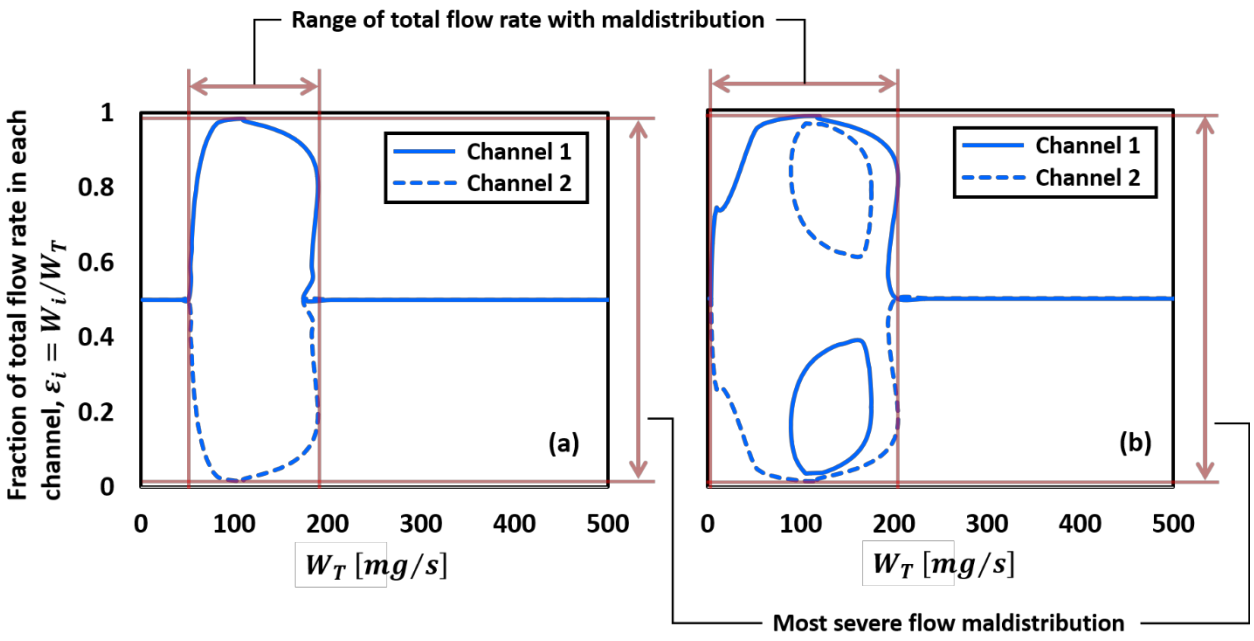

Fig. 3. Flow distribution diagrams showing the relative flow rate fraction as a function of the total flow rate for the two characteristic flow distribution behaviors: (a) a single continuous curve (where the top half of the curve represents channel 1 with excess flow, while the bottom half represents the flow-starved channel 2); and (b) two isolated curves: for the outer flow distribution curve, channel 1 has excess flow while channel 2 is starved, and for the inner curve, channel 2 has excess flow while channel 1 is starved.

For the set of parameters listed in Table 1, two characteristic flow distribution diagrams are possible under uneven heating conditions. First, as shown in Fig. 3a, a single loop where all possible steady-state flow distributions are joined by a continuous curve. Second, as shown in Fig. 3b, the flow distribution diagram often separates into two isolated curves, a big outer loop and smaller inner loops, as reported in Ref. [20]. The outer loops are connected continuously across all flow rates. The smaller loops are isolated curves, meaning that the channel load curves are non-identical, which physically indicates that the operating points lying on the inner loops cannot be reached continuously via a stable flow path. In practice, to enable the system to shift from the outer loop to the inner loops, an external influence such as the temporary throttling of the inlet valve would be required [20]. During such an operation, as the system can transiently jump from the outer to the inner curve or vice-versa taking a path along unstable operating conditions, the flow within the channels experiences an excursion and the distribution is swapped between the channels. This is evident from the symmetry of the loops with respect to the uniform flow

distribution case. With this basic introduction of the two types of flow distribution diagrams, the effect of uneven heating on the flow distribution behavior is discussed in the following sections.

3.2 Flow distribution behavior under lateral uneven heating

Figure 4 shows the flow distribution visualized as the relative flow rate fraction versus the total flow rate. In Fig. 4, each row demonstrates the effect of increasing thermal conductance (left to right) at a given total input power, while each column demonstrates the effect of increasing input power (top to bottom) at a given value of thermal conductance. The flow rate range is kept the same across all plots. In each plot, the black curve represents the baseline case of even heating, while the blue curves represent the flow distribution behavior at different levels of lateral uneven heating. The solid lines represent the flow rate fraction in channel 1 while the dotted lines represent the flow rate fraction in channel 2. The degree of lateral uneven heating to which the channels are subjected for a given total input power is quantified by comparing the relative input powers to the channels, through a lateral unevenness parameter:

$$\varphi = \frac{P_{high} - P_{low}}{P_{T,in}}, \quad 0 \leq \varphi \leq 1 \tag{4}$$

where $P_{T,in}$ $(= P_{high} + P_{low})$ refers to the total power input to the channel heaters. The subscripts high and low refer to the channels receiving the higher and the lower portions of the input power, respectively. With this definition, $\varphi = 0$ corresponds to a case of uniform heating case while $\varphi = 1$ represents a case of extreme non-uniform heating where all heat is fed into one channel. The results in Fig. 4 are shown for three levels of lateral non-uniform heating ($\varphi = 0$, 0.5, and 1) at three different total power inputs (2.2 W, 4.4 W and 8.8 W).

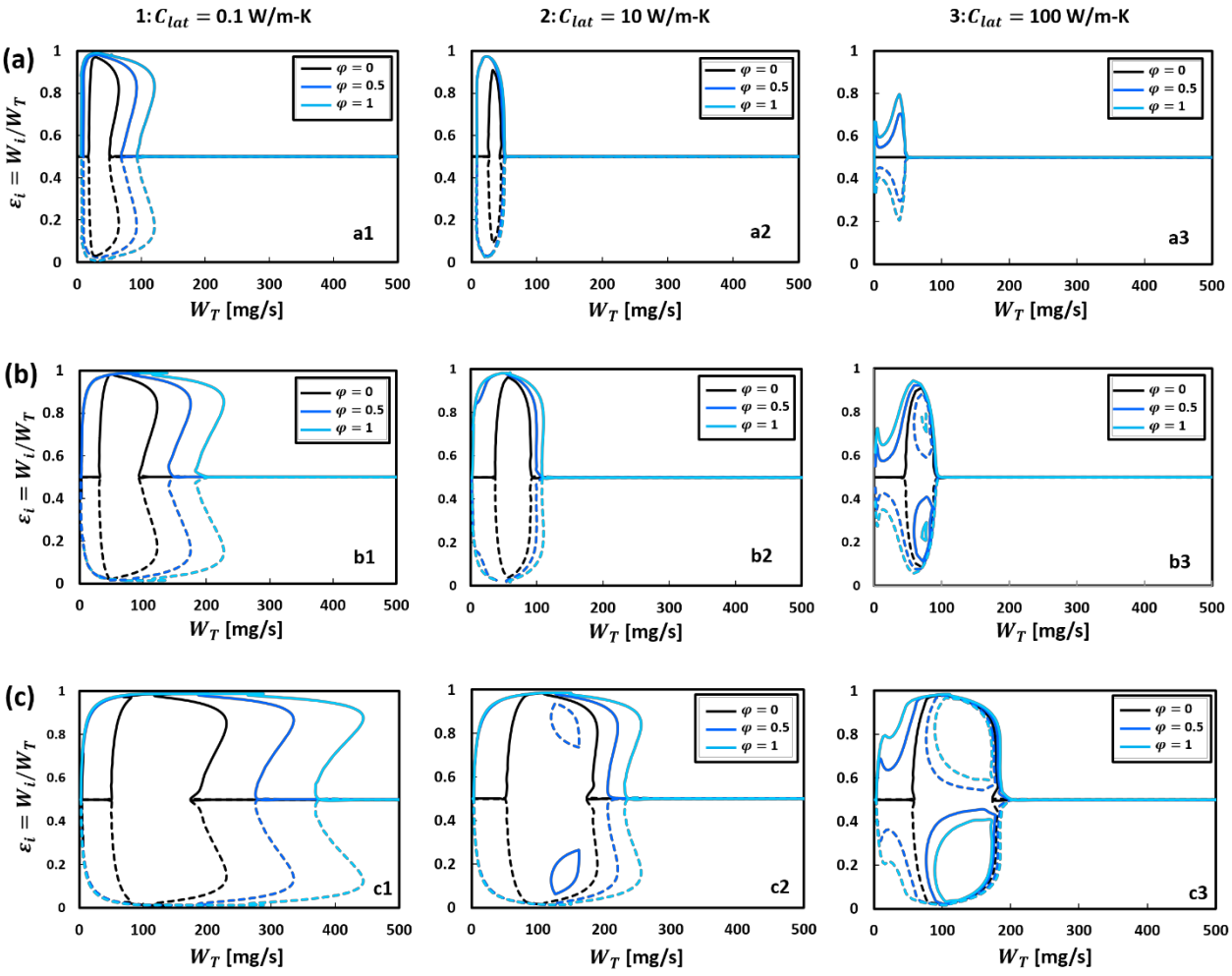

Fig. 4. Relative flow rate distribution, shown as the flow rate fraction ($\varepsilon_i = W_i/W_T$) versus total flow rate W_T for two identical parallel microchannels (parameters in Table 1) subjected to varying degrees of lateral uneven heating. The results are shown for different magnitudes of total input power: (a) $P_{T,in} = 2.2$ W (top row), (b) $P_{T,in} = 4.4$ W (middle row), and (c) $P_{T,in} = 8.8$ W (bottom row) at different values of thermal conductance between the channels: $C_{lat} = 0.1$ W/m-K (left column), $C_{lat} = 10$ W/m-K (middle column) and $C_{lat} = 100$ W/m-K (right column).

In comparing the even heating versus lateral uneven heating cases at the lowest thermal conductance between the channels $C_{lat} = 0.1$ W/m-K (left) (Figure 4, left column), it is apparent that the flow distribution is adversely impacted by lateral uneven heating. For example, consider Fig. 4c1 and compare the extreme cases $\varphi = 0$ and $\varphi = 1$. First, the range of total flow rates experiencing flow maldistribution is significantly larger for the latter. Maldistribution occurs at

total flow rates of 50 mg/s to 230 mg/s for the uniform heating case, while this range is much larger in the lateral uneven heating case, extending from 2 mg/s to 445 mg/s. Second, the severity of flow maldistribution is higher at any given total flow rate (except for a small range between 88 mg/s to 120 mg/s), i.e., the flow rate fraction of the flow-starved channel is always lower in the uneven heating case compared to the even heating case. Focusing on a specific total flow rate of 230 mg/s, for extreme uneven heating ($\varphi = 1$) the flow rate fraction can be as low as 0.013 compared to 0.15 in the even heating case. Third, the range of total flow rates over which the flow maldistribution is most severe is markedly larger. We identify this range as one with the highest flow rate fraction in channel 1 and lowest in channel 2. In the even heating case, the most severe flow maldistribution (98.7% in channel 1 and 1.3% in channel 2) occurs for total flow rates between 90 mg/s to 140 mg/s, a much smaller range compared to 75 mg/s to 295 mg/s in the uneven heating case. In summary, while both the even and lateral uneven heating cases display significant flow rate imbalances when there is low lateral thermal conductance between the channels, the flow maldistribution is markedly worse for the non-uniform heating, as indicated by the broadened flow distribution curves.

The effect of an increasing degree of lateral non-uniform heating can be similarly understood based on the three metrics for flow maldistribution, *i.e.*, the range of total flow rates with flow maldistribution, the severity of flow maldistribution, and the total flow rate range with the most severe flow maldistribution. Figures 4a1, b1 and c1 show that when the channels are poorly thermally connected ($C_{lat} = 0.1$ W/m-K), which is representative of thermally isolated channels, the flow maldistribution worsens with increasing degree of lateral uneven heating (from $\varphi = 0$ to $\varphi = 1$). For example, comparing the $\varphi = 0.5$ to $\varphi = 1$ curves in Fig. 4c1 shows that the range of total flow rate with maldistributed flow as well as the total flow rate with most severe flow maldistribution extends up to 443 mg/s and 220 mg/s respectively for $\varphi = 1$, which are significantly larger compared to 333 mg/s and 115 mg/s respectively for $\varphi = 0.5$. Similarly, the severity of flow maldistribution at any given total flow rate is higher at $\varphi = 1$ compared to $\varphi = 0.5$. Overall, in thermally isolated channels, the range of total flow rate with flow maldistribution, the severity of flow maldistribution and the range of total flow rate with most severe flow maldistribution increase monotonically with increasing degree of lateral uneven heating.

The effect of the total heat load to the channels on the flow distribution behavior can be assessed by comparing the top (2.2 W), middle (4.4 W), and the bottom (8.8 W) rows in Fig. 4. The relative extent of the total flow rate range and the severity of flow maldistribution increases with increasing total heat load. An increase in the total flow rate range is seen most prominently when comparing the flow distribution curves of Figures 4 a1, b1 and c1 for low lateral thermal conductance. Focusing on flow distribution curves with a fixed value of unevenness parameter $\varphi = 1$, the flow rate range with maldistributed flow is observed to increase ~3.8 times on increasing the heat load from 2.2 W to 8.8 W. However, at the low lateral thermal conductance ($C_{lat} = 0.1$ W/m-K), the severity of the flow maldistribution is always extreme. The increase in the severity of flow maldistribution with increasing total power is seen more distinctly in comparing Figures 4a3, b3 and c3. For $\varphi = 1$, the most severe flow distribution has a flow rate fraction of 0.2 in the flow-starved channel at 2.2 W, decreasing to 0.016 at 8.8 W for this highest value of lateral thermal conductance ($C_{lat} = 100$ W/m-K). The most severe flow distribution worsens with increasing total input power because, at a given total flow rate and inlet subcooling, the absolute value of heat load to which each channel is subjected increases for a given value of unevenness parameter. For example, for $\varphi = 0.5$, channel 1 and channel 2 would be subjected to head loads of 1.65 W and 0.55 W respectively at $P_{T,in} = 2.2$ W, while for the same $\varphi = 0.5$ at $P_{T,in} = 8.8$ W, the corresponding values are 6.6 W and 2.2 W, respectively. Because of higher input power, the channel has a higher vapor quality and incurs an increased hydraulic resistance, thereby resulting in worsening of the most severe flow distribution with increasing input power.

The extent to which lateral uneven heating affects the flow distribution also depends on the strength of thermal coupling between the channels. Fig. 4 shows the effect of increasing thermal conductance between the channels on the flow distribution behavior. From left to right in Fig. 4 the thermal conductance varies by three orders of magnitude from $C_{lat} = 0.1$ W/m-K to $C_{lat} = 100$ W/m-K. This encompasses the range of channel-to-channel thermal conductance values that could occur due to substrate conduction in a typical microchannel heat sink for electronics cooling applications. It is clear from Fig. 4 that thermal conductance alleviates the flow rate imbalance between channels. Also, the worsening of flow maldistribution with an increase in the unevenness of heating dampens as the thermal conductance between the channels is increased. The role of thermal conductance in mitigating flow maldistribution is due to the possibility of heat redistribution between the channels via the walls and the substrate, as explained in our previous

study [14]. This means that the channel which receives excess flow will also share a larger portion of the total heat load, while the flow-starved channel will share a smaller portion of the total heat load. This aids in reducing the vapor quality difference between the channels and equalizing their hydraulic resistances, thereby resulting in reduced flow maldistribution. In contrast, when the channels are weakly thermally connected, even when the flow rate between the channels is severely maldistributed the channels tend to share their respective heat loads as no channel-to-channel heat exchange is possible, and therefore, the severity of flow maldistribution increases with increasing degree of uneven heating.

Interestingly, for each total heat load there exists a certain threshold thermal conductance at which the effect of degree of lateral uneven heating on the flow distribution starts to vanish. This is indicated by the collapsing of the different flow distribution curves, to the point where all the curves start to overlap. Further, this value of thermal conductance increases with increasing total heat load. For example, at 2.2 W and 4.4 W the curves nearly collapse at $C_{lat} = 10$ W/m-K, but at 8.8 W it requires a higher conductance of $C_{lat} = 100$ W/m-K before a similar collapse is observed. While the increments in the thermal conductance plotted in Fig. 4 are relatively large, for a given total heat load, this threshold value can be determined by progressively making incremental changes in thermal conductance for each value of lateral unevenness parameter φ. Beyond this value, the flow distribution curves are almost indistinguishable, meaning that the flow distribution behavior at any degree of lateral uneven heating is nearly identical and same as that under the even heating conditions. Increasing the strength of thermal connectedness between the channels is thereby an effective method by which the flow maldistribution under lateral uneven heating conditions can be mitigated, at least to the level of flow maldistribution under even heating conditions.

4. Comparison to experiments

In this section, experimental results for both thermally isolated and thermally coupled channels subject to extreme lateral uneven heating are presented and compared with the model predictions. This comparison allows an assessment of the suitability of the model for predicting two-phase flow distribution in parallel microchannels experiencing boiling under lateral uneven heating conditions. The experimental results are presented for a case of thermally isolated and

coupled channels subjected to extreme lateral uneven heating ($\varphi = 1$) at increasing power levels in the range $P_{T,in}$ = 2.6 – 8.5 W and compared with the even heating case ($\varphi = 0$). Subsequently, the experimental data are compared with the model-predicted flow distributions under matching conditions. Other operating parameters and the operating conditions of the experiments that are used as inputs to the model are listed in Table 1. The lateral thermal conductance of the thermally isolated and the thermally coupled channels is taken to be $C_{lat} = 0.36$ W/K and 18.5 W/K, respectively. For the thermally coupled channels, the value of C_{lat} is estimated using a 1D thermal resistance network, while for the thermally isolated channels it is determined through calibration with the model, as described in our previous study [14].

4.1 Experimental methods

A detailed description of the test section and the two-phase flow loop used for the experiments can be found in Refs. [13, 14]. In this section, the key features of the experimental facility are summarized and the unique experimental procedures for measuring flow maldistribution under extreme lateral uneven heating conditions are discussed.

The test section is the same as that described in Refs. [13, 14], and therefore, only key details are included here for completeness. A photograph of the test section is shown in Fig. 5, with the transparent top cover plate removed. The test section consists of a bottom base made of polyether ether ketone (PEEK) and a polycarbonate top cover plate vertically stacked and sealed together with a laser-cut insulating silicon rubber sheet to complete the assembly. The middle section made of PEEK contains the parallel flow paths, which comprise three sub-sections in the flow direction: an upstream unheated section, the heated copper blocks, and a downstream unheated section. The de-ionized (DI) water enters the inlet plenum in the upstream unheated section, divides into two microchannels and then exits the test section via the outlet plenum in the downstream unheated section. The square microchannels (1 mm × 1 mm) are milled in a single pass through the PEEK and copper sections, and their total length is divided into two equal halves. The first half lies in the upstream unheated PEEK section, which remains in a single-phase flow regime and is utilized to measure the pressure drop separately in each channel. The single-phase pressure drop is measured using differential pressure transducers (0-249 Pa PX154-001DI Wet-Wet type, Omega Engineering; ±2% full scale), which is then used to determine the flow rate in each channel and quantify flow maldistribution. For flow rate measurement in each channel, the

current output from the differential pressure transducers is converted to the flow rate via a calibration to the liquid flow meter that measures the total flow rate W_T $(= W_1 + W_2)$. A linear fit of flow rate versus current output is obtained for both the transducers, which is used to convert the measured signal to the channel flow rate. A combined linear fit for both the differential pressure transducers is obtained as: $W_i = 2.108I_i - 8.433$, where W_i is the flow rate, and I_i is the measured transducer output current in milliamperes (mA) for a given channel (i =1, 2 for channels 1 and 2, respectively). For all tests, the flow distribution is represented as the fraction of the total flow rate going into each individual channel $\varepsilon_i = W_i/W_T$ such that the sum of the flow rate fractions is unity. The flow is then said to be uniformly distributed when ε_i = 0.5, and maldistributed otherwise. In the maldistributed state $\varepsilon_1 > 0.5$ for the channel that receives excess flow while $\varepsilon_2 < 0.5$ for the other channel that is starved of flow. To determine the flow maldistribution resulting from lateral uneven heating, the flow rate measurement from the channel in the single-phase liquid regime that receives excess flow is subtracted from the total flow rate W_T to find the flow rate in the flow-starved channel.

The second half of the channel length lies in the heated copper blocks with the heaters installed beneath the blocks. A portion of the power applied to the channel is lost to the ambient and not absorbed by the fluid. Therefore, a calibration of the heat loss is performed as detailed in our previous studies [13, 14]. Power to the channel blocks can be controlled separately through their respective heater power supplies to achieve uneven heating conditions. In the thermally isolated configuration, a 1 mm air gap that runs across the entire depth of the test section and for ~90% of the total channel length is maintained between the copper blocks, while in the thermally coupled configuration, both the channels are milled into a single copper block while maintaining the same pitch, which ensures that a strong channel-to-channel thermal interaction exists via heat conduction through solid copper.

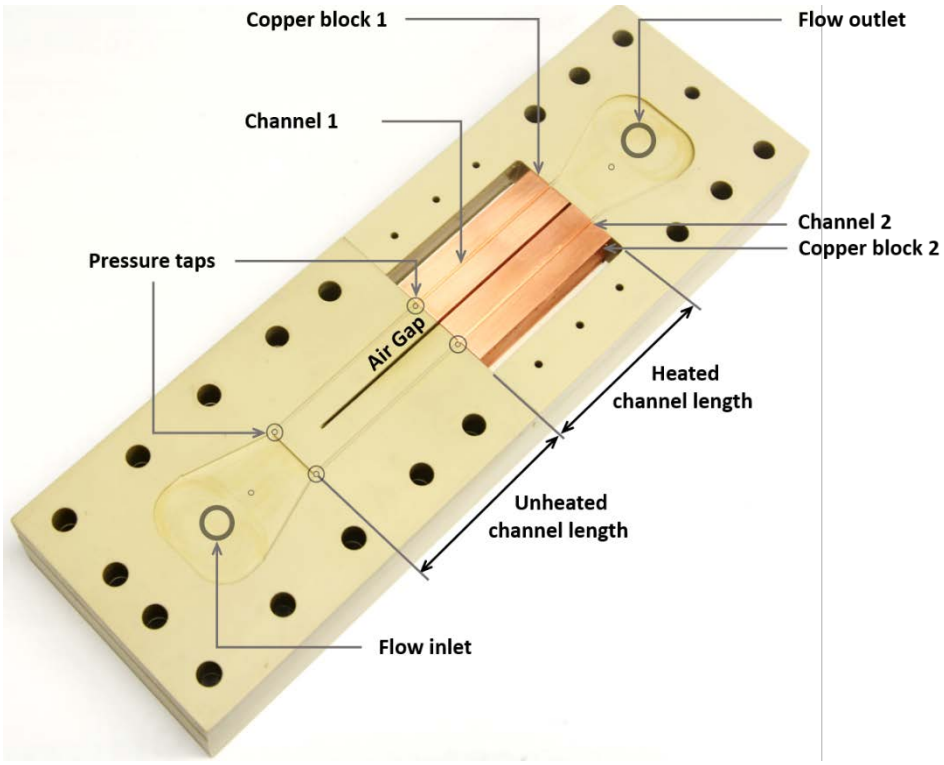

Fig. 5. Photograph of the test section with two parallel microchannels in the thermally isolated configuration and the key components annotated. The location of pressure taps for measuring pressure drop in the upstream unheated length of each channel are marked; these are used for direct measurement of the flow maldistribution induced by lateral uneven heating. In thermally coupled channels, the two channels are cut into the same solid copper block such that there is no air gap.

The experimental procedure for measuring flow maldistribution is as reported in our previous work [13, 14]. Experiments are conducted at a single, constant total inlet mass flux of 150 kg/m^2-s. DI water is circulated through the flow loop at this constant flow rate and preheated to 88.5 °C at the test section inlet, which corresponds to a subcooling of 11.6 °C corresponding to the test section outlet pressure (104.4 kPa). The expandable reservoir is used to set the system at atmospheric pressure prior to turning on the heaters. An even heating condition with $\varphi = 0$ is achieved by powering two separate aluminum nitride heaters (582 W CER-1-01-00003, Watlow) simultaneously; each is mounted underneath the channel blocks. A lateral uneven heating condition with a maximum degree of unevenness ($\varphi = 1$) is achieved by powering the heater underneath one of the channel blocks while keeping the other switched-off. To further study the effect of increasing total power on the flow maldistribution, the power input into the heated channel

is increased in steps from 2.6 W to 8.5 W, and the flow distribution is measured at each power level. This input power is the power absorbed by the fluid flowing in the channel after accounting for heat loss to the ambient (*i.e.*, by subtracting the power loss to the ambient from the power applied to the heaters). It is important to note that when comparing the flow distribution behavior under even heating and lateral uneven heating cases, it is done at the same fixed total input power in both cases.

4.2 Effect of lateral uneven heating on the flow distribution behavior

Figure 6 shows the experimentally measured relative flow rate distribution between thermally isolated channels as a function of increasing total heat load under even and lateral uneven heating conditions. At the lowest input power of $P_{T,\,in}$ = 2.7 W, when both the channels are in the single-phase liquid regime, the total flow rate is distributed equally ($\varepsilon_1 = \varepsilon_2 = 0.5$) between the channels under both even and uneven heating conditions. This is seen in Fig. 6 as the overlapping of data points at $P_{T,\,in}$ = 2.7 W, each with a flow rate fraction of 0.5. With an increase in the input power to $P_{T,\,in}$ = 4.4 W, a difference between the flow rate distributions in the two cases emerges. In the even heating case, the flow remains in the single-phase liquid regime in both channels with even distribution. In the uneven heating case, boiling initiates in channel 2 while channel 1 remains in the single-phase regime. Boiling in channel 2 leads to vapor generation which increases the pressure drop across the channel, thereby diverting most of the flow to channel 1. By this mechanism, the total flow rate is maldistributed between the channels, where channel 1 receives excess flow ($\varepsilon_1 = 0.9$) and channel 2 (the boiling channel) is starved of flow ($\varepsilon_2 = 0.1$). A further increase in the power to $P_{T,\,in}$ = 7.6 W induces the flow maldistribution under even heating as well. Clearly, the range of input power over which the flow is maldistributed, and the severity at a given power, is larger for the uneven heating conditions. Because the heat exchange between channels is restricted by thermally isolating them, the entire heat load is shared by one channel (for $\varphi = 1$) in the uneven heating case compared to the equal sharing in the even heating case. This leads to comparatively more vapor generation and a higher pressure drop across the boiling channel, and therefore, a more severe flow maldistribution compared to the even heating conditions. For this same reason, the flow maldistribution under both the heating conditions also worsens with

increasing power. Therefore, when the channels are thermally isolated or weakly thermally coupled, the flow is always more severely maldistributed under uneven heating conditions than in the even heating case at any given input power, as indicated by the model predictions in Fig 4.

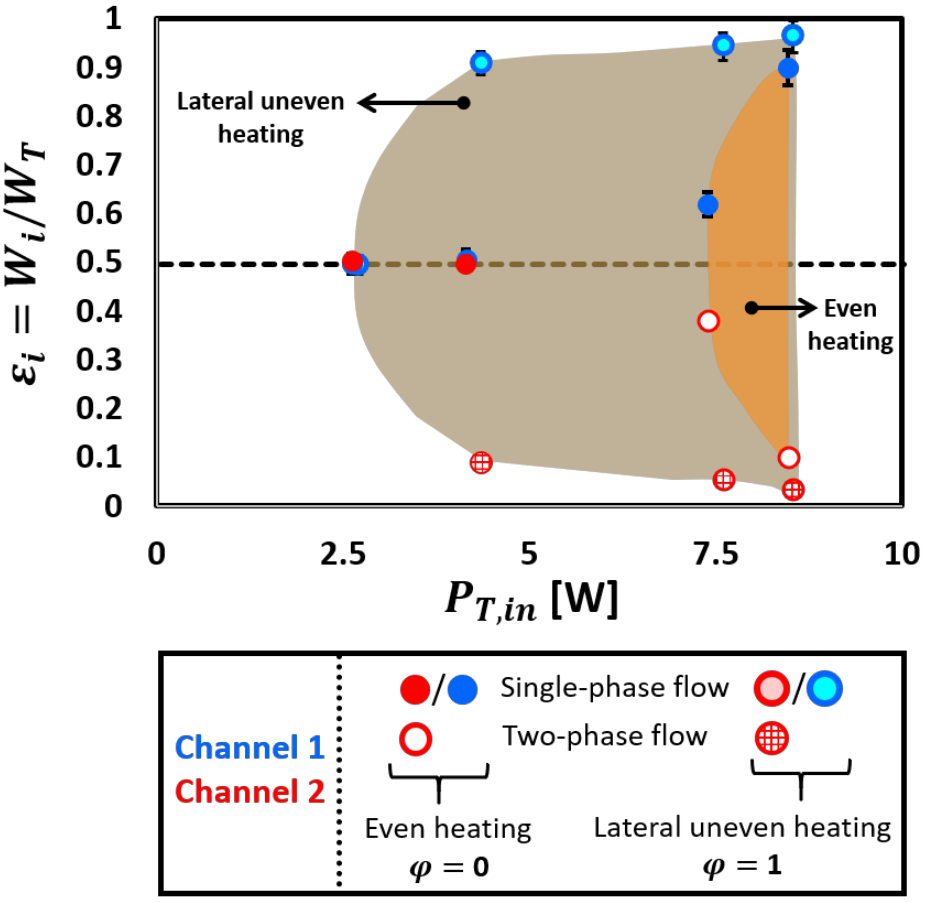

Fig. 6. Comparison of the experimentally measured relative flow distribution characteristics, shown as flow rate fraction, of the thermally isolated parallel channels under even heating ($\varphi = 0$) and lateral uneven heating conditions ($\varphi = 1$) with increasing power. The black horizontal dashed line represents an even flow distribution between the channels. The flow regime in each channel is denoted by the marker type as detailed in the legend.

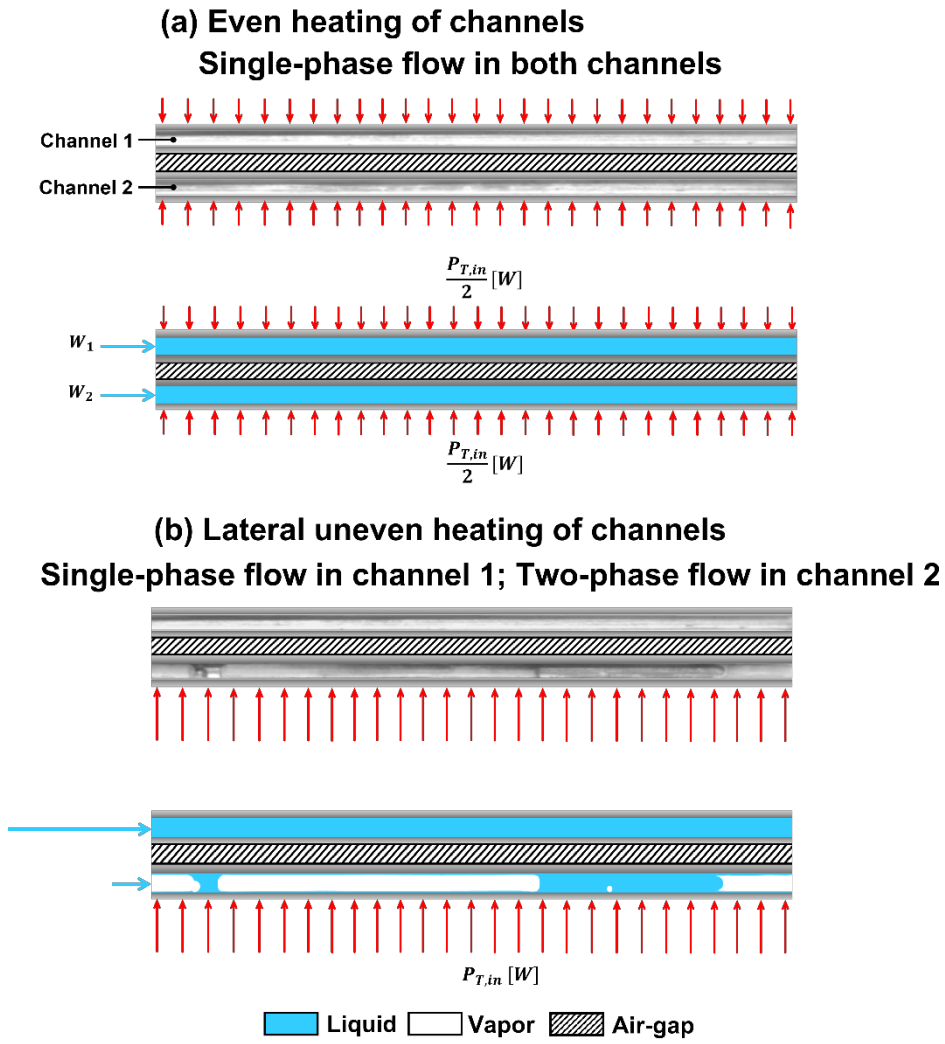

Fig. 7. Flow visualization images and the accompanying schematic representations of the flow regime observed in each channel for thermally isolated configuration, subject to different heating conditions: (a) even heating, and (b) lateral uneven heating at a total input power of $P_{T,\,in}$ = 4.4 W. The flow direction is from left to right.

The flow in both the microchannels is visualized under even and extreme lateral uneven heating ($\varphi = 1$) at a total input power of $P_{T,\,in}$ = 4.4 W. Fig. 7 shows selected flow visualization images obtained by the high-speed camera and an accompanying schematic representation of the flow regime in the two parallel channels. The flow direction is from left to right. The channels and the air gap for thermal isolation (hashed region) are marked. The viewing region covers ~90% of the heated channel length. The flow rate through each channel is qualitatively represented by the length of the arrow near the channel inlet. The images allow visual detection of the flow

morphology in each channel when flow maldistribution exists and support the trend shown in Fig. 6. That is, at a given total input power of $P_{T,\,in}$ = 4.4 W and above, the flow maldistribution between the channels is more severe under lateral uneven heating compared to the even heating condition.

4.3 Comparison with model predictions

Predictions from the two-phase flow distribution model summarized in Section 2 are now compared against the experimental flow distribution data for thermally isolated and thermally coupled microchannels subjected to lateral uneven heating. The parameters and the operating conditions used as inputs to the model match those listed in Table 1. Note that while the modeling results presented in Section 3.2 show the flow maldistribution predictions over a large range of flow rates, the experiments were performed at a fixed total flow rate of 150 mg/s at which increasing power input levels were studied. Accordingly, the model predictions are obtained in similar fashion with increasing input power. Because the flow distribution behavior is a function of inlet sub-cooling, total mass flow rate, and system pressure, the sensitivity of the model predictions to the changes in these key input variables is assessed by calculating the bounds of the model output (in terms of flow rate fraction) for a variation in each of the input variables, within their measurement uncertainty. The model output bounds are estimated for a change of ± 0.5 °C in inlet sub-cooling, ± 3 mg/s in total mass flow rate, and ± 1.2 kPa in system pressure. The bounds corresponding to these uncertainties in the model input variables are indicated by the error bars in Fig. 8 for the model-predicted flow distribution at each input power level.

The relative flow distribution behavior from the experiments and predictions is shown in Fig. 8. Over the entire range of input power, the magnitude of predicted flow rate fractions is in excellent agreement with the measurements. In thermally isolated channels (see Fig. 8a), for $P_{T,\,in}$ = 2.7 W, where both the channels are in the single-phase liquid regime, the predictions of an equal flow rate fraction match the experiments. At $P_{T,\,in}$ = 4.35 W, when boiling occurs in channel 2 and causes flow maldistribution, the model accurately predicts the appearance of a significant flow imbalance with only slight quantitative differences from the experiments. Over the range of input power where flow maldistribution is observed, the maximum absolute error in the predicted flow

rate fraction of channel 1 is ~4.5% compared to the experiments at the highest tested input power of $P_{T,\,in}$ = 8.5 W. For thermally coupled channels (see Fig. 8b), the results also capture the influence of lateral wall conduction in dampening flow maldistribution under lateral uneven heating conditions. While flow maldistribution between the two channels is observed under uneven heating for both the isolated and coupled cases, it is much less severe in the coupled case. Correspondingly, the maximum severity of flow maldistribution is higher in the isolated case (96.5 % in channel 1 and 3.5% in channel 2 at $P_{T,in} = 8.5$ W) compared to the coupled case (86 % in channel 1 and 14 % in channel 2 at $P_{T,in} = 8.5$ W). This agreement with the experiments firmly establishes the behavioral trends predicted by the model, namely, a strong thermal coupling leads to a more uniform flow distribution under uneven heating conditions.

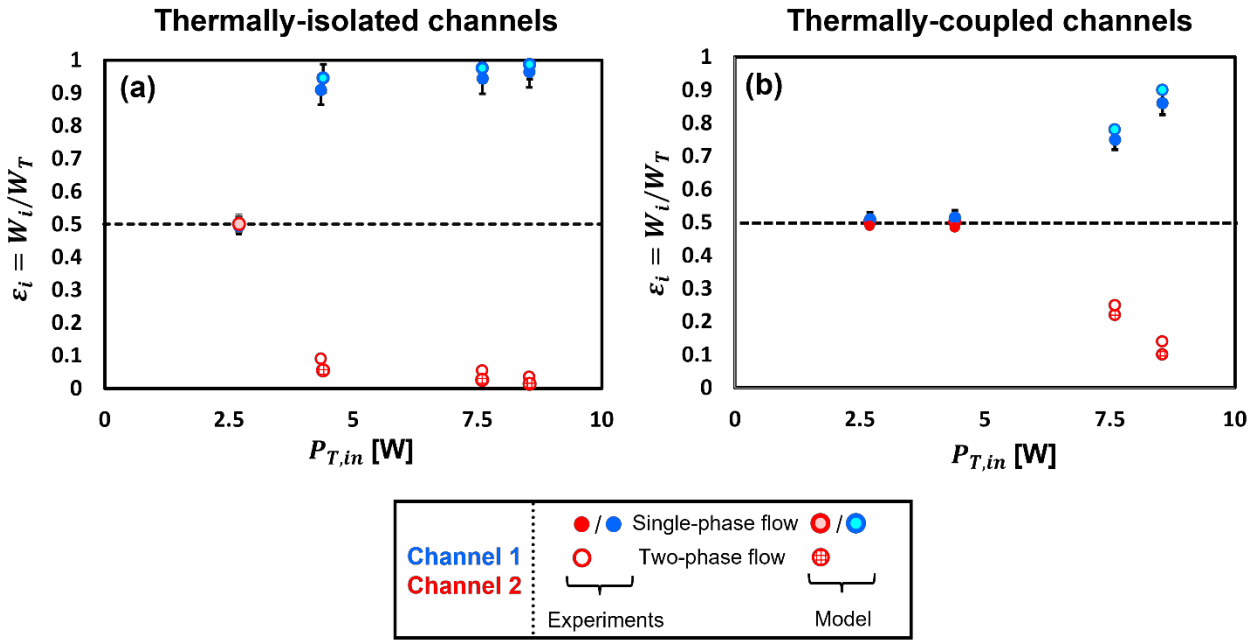

Fig. 8. Comparison of the relative flow rate distribution, shown as flow rate fraction with increasing power, between the experiments and the model predictions for parallel microchannels subjected to extreme lateral uneven heating conditions ($\varphi = 1$): (a) thermally isolated channels, and (b) thermally coupled channels. The flow regime in each channel is denoted by the marker type as detailed in the legend.

5. Conclusions

The effect of lateral uneven heating conditions on the flow distribution behavior between parallel microchannels undergoing boiling is investigated, along with a comparison to the known characteristic behavior under even heating conditions. The severity of flow maldistribution under such uneven heating conditions is quantified, and the following key conclusions are drawn from the present study:

- Flow maldistribution under lateral uneven heating conditions is generally more severe compared to even heating conditions.
- The severity of flow maldistribution increases with the degree of lateral uneven heating in terms of following three metrics: the range of flow rates over which flow maldistribution occurs, the maximum difference in the flow rate fraction between the channels, and the range of total flow rate with most severe flow maldistribution. Under extreme lateral uneven heating where the entire heat load is applied to one channel, the range of total flow rate with flow maldistribution is 2 mg/s to 445 mg/s, while for the uniform heating case the range is much narrower (50 mg/s to 230 mg/s). The flow is also highly maldistributed such that the flow-starved channel receives just 1.3% of the total flow rate compared to 15% in the even heating case. Further, under extreme uneven heating, the range of total flow rates with the most severe flow maldistribution (98.7% in channel 1 and 1.3% in channel 2) is much larger (75 mg/s to 295 mg/s) compared to 90 mg/s to 140 mg/s in the even heating case.
- Channel-to-channel thermal conduction via the channel walls and the substrate plays a vital role in mitigating flow maldistribution under uneven heating conditions by enabling heat redistribution. The flow maldistribution can be dampened at least to the level of even heating conditions by increasing the thermal connectedness between the channels. However, an increase in thermal conductance between the channels reduces the severity of flow maldistribution only up to a certain threshold, beyond which no further reduction is observed. This is especially true at high heat loads exhibiting the most severe maldistribution.

- Experimental measurements of the flow maldistribution in both thermally isolated and thermally coupled microchannels were performed under extreme lateral uneven heating conditions, and the growing severity of maldistribution with increasing input power demonstrated experimentally for the first time. It was also demonstrated that the range of input power over which the flow maldistribution is observed is shorter in case of thermally coupled channels compared to the isolated channels, which confirms the influence of thermal coupling in dampening flow maldistribution under uneven heating conditions.
- The experimentally measured flow distribution under extreme uneven heating is shown to quantitatively match the predictions of the two-phase flow distribution model.

Acknowledgements

This material is based upon work supported by Ford Motor Company through the University Research Program (URP). Special thanks to Dr. Edward Jih at Ford Research & Advanced Engineering (R&AE) for technical discussions related to this work. The first author would like to acknowledge the Science and Engineering Research Board (SERB) and Indo-US Science and Technology Forum (IUSSTF) for support through the SERB Indo-US Postdoctoral Fellowship.

References

[1] Hamann, H. F., Weger, A., Lacey, J. A., Hu, Z., Bose, P., Cohen, E., & Wakil, J. (2006). Hotspot-limited microprocessors: Direct temperature and power distribution measurements. *IEEE Journal of Solid-State Circuits*, *42*(1), 56-65.

[2] Cho, E. S., Choi, J. W., Yoon, J. S., & Kim, M. S. (2010). Experimental study on microchannel heat sinks considering mass flow distribution with non-uniform heat flux conditions. *International Journal of Heat and Mass Transfer*, *53*(9-10), 2159-2168.

[3] Costa-Patry, E. (2011). Cooling high heat flux micro-electronic systems using refrigerants in high aspect ratio multi-microchannel evaporators. *EPFL, Lausanne*, Ph.D. Thesis, 230.

[4] Alam, T., Lee, P. S., Yap, C. R., & Jin, L. (2013). A comparative study of flow boiling heat transfer and pressure drop characteristics in microgap and microchannel heat sink and an evaluation of microgap heat sink for hotspot mitigation. *International Journal of Heat and Mass Transfer*, *58*(1-2), 335-347.

[5] Bogojevic, D., Sefiane, K., Walton, A. J., Lin, H., Cummins, G., Kenning, D. B. R., & Karayiannis, T. G. (2011). Experimental investigation of non-uniform heating effect on flow boiling instabilities in a microchannel-based heat sink. *International Journal of Thermal Sciences*, *50*(3), 309-324.

[6] Ritchey, S. N., Weibel, J. A., & Garimella, S. V. (2014). Local measurement of flow boiling heat transfer in an array of non-uniformly heated microchannels. *International Journal of Heat and Mass Transfer*, *71*, 206-216.

[7] Sarangi, R. K., Bhattacharya, A., & Prasher, R. S. (2009). Numerical modelling of boiling heat transfer in microchannels. *Applied Thermal Engineering*, *29*(2-3), 300-309.

[8] Revellin, R., & Thome, J. R. (2008). A theoretical model for the prediction of the critical heat flux in heated microchannels. *International Journal of Heat and Mass Transfer*, 51(5-6), 1216-1225.

[9] Revellin, R., QuibÉn, J. M., Bonjour, J., & Thome, J. R. (2008). Effect of local hot spots on the maximum dissipation rates during flow boiling in a microchannel. *IEEE Transactions on Components and Packaging Technologies*, *31*(2), 407-416.

[10] Miler, J. L., Flynn, R., Refai-Ahmed, G., Touzelbaev, M., David, M., Steinbrenner, J., & Goodson, K. E. (2009, January). Effects of transient heating on two-phase flow response in microchannel heat exchangers. In *International Electronic Packaging Technical Conference and Exhibition* (Vol. 43604, pp. 563-569).

[11] Kingston, T. A., Weibel, J. A., & Garimella, S. V. (2020). Time-resolved characterization of microchannel flow boiling during transient heating: Part 1–Dynamic response to a single heat flux pulse. *International Journal of Heat and Mass Transfer*, 154, 119643.

[12] Kingston, T. A., Weibel, J. A., & Garimella, S. V. (2020). Time-resolved characterization of microchannel flow boiling during transient heating: Part 2–Dynamic response to time-periodic heat flux pulses. *International Journal of Heat and Mass Transfer*, 154, 119686.

[13] Miglani, A., Weibel, J. A., & Garimella, S. V. (2021). Measurement of flow maldistribution induced by the Ledinegg instability during boiling in thermally isolated parallel microchannels. *International Journal of Multiphase Flow*, *139*, 103644.

[14] Miglani, A., Weibel, J. A., & Garimella, S. V. (2021). An experimental investigation of the effect of thermal coupling between parallel microchannels undergoing boiling on the Ledinegg instability-induced flow maldistribution. *International Journal of Multiphase Flow*, *139*, 103536.

[15] Van Oevelen, T., Weibel, J. A., & Garimella, S. V. (2018). The effect of lateral thermal coupling between parallel microchannels on two-phase flow distribution. *International Journal of Heat and Mass Transfer*, *124*, 769-781.

[16] Van Oevelen, T., Weibel, J. A., & Garimella, S. V. (2017). Predicting two-phase flow distribution and stability in systems with many parallel heated channels. *International Journal of Heat and Mass Transfer*, *107*, 557-571.

[17] Cho, E. S., Choi, J. W., Yoon, J. S., & Kim, M. S. (2010). Experimental study on microchannel heat sinks considering mass flow distribution with non-uniform heat flux conditions. *International Journal of Heat and Mass Transfer*, *53*(9-10), 2159-2168.

[18] Flynn, R. D., Fogg, D. W., Koo, J. M., Cheng, C. H., & Goodson, K. E. (2006, January). Boiling flow interaction between two parallel microchannels. In *ASME International Mechanical Engineering Congress and Exposition* (Vol. 47853, pp. 317-322).

[19] Flynn, R., Cheng, C. H., & Goodson, K. (2007, January). Decoupled thermal and fluidic effects on hotspot cooling in a boiling flow microchannel heat sink. In *International Electronic Packaging Technical Conference and Exhibition* (Vol. 42770, pp. 179-184).

[20] Akagawa, K., Kono, M., Sakaguchi, T., & Nishimura, M. (1971). Study on distribution of flow rates and flow stabilities in parallel long evaporators. *Bulletin of JSME*, *14*(74), 837-848.

[21] Minzer, U., Barnea, D., & Taitel, Y. (2004). Evaporation in parallel pipes—splitting characteristics. *International journal of multiphase flow*, *30*(7-8), 763-777.

[22] Minzer, U., Barnea, D., & Taitel, Y. (2006). Flow rate distribution in evaporating parallel pipes—modeling and experimental. *Chemical Engineering Science*, *61*(22), 7249-7259.

[23] Lockhart, R. W. (1949). Proposed correlation of data for isothermal two-phase, two-component flow in pipes. *Chem. Eng. Prog.*, *45*, 39-48.